High-capacity $FeTiO_3$/C negative electrode for sodium-ion batteries with ultralong cycle life

Changsheng Ding,[a] Toshiyuki Nohira[b] and Rika Hagiwara[a]

[a] Graduate School of Energy Science, Kyoto University, Sakyo-ku, Kyoto 606-8501, Japan

[b] Institute of Advanced Energy, Kyoto University, Uji, Kyoto 611-0011, Japan

* Corresponding authors. Tel.: +81 75 753 5822; Fax: +81 75 753 5906.

E-mail addresses: nohira.toshiyuki.8r@kyoto-u.ac.jp (T. Nohira)

hagiwara@energy.kyoto-u.ac.jp (R. Hagiwara)

Abstract

The development of electrode materials which improve both the energy density and cycle life is one of the most challenging issues facing the practical application of sodium-ion batteries today. In this work, $FeTiO_3$/C nanoparticles are synthesized as negative electrode materials for sodium-ion batteries. The electrochemical performance and charge-discharge mechanism of the $FeTiO_3$/C negative electrode are investigated in an ionic liquid electrolyte at 90 °C. The $FeTiO_3$/C negative electrode delivers a high reversible capacity of 403 mAh g^{-1} at a current rate of 10 mA g^{-1}, and exhibits high rate capability and excellent cycling stability for up to 2000 cycles**.** The results indicate that $FeTiO_3$/C is a promising negative electrode material for sodium-ion batteries.

Keywords: Sodium ion batteries; Negative electrode materials; High capacity; High stability; Charge-discharge mechanism

1. Introduction

Development of renewable energy generation and electric vehicles (EVs) has resulted in a rapid increase in the demand for large-scale energy storage systems. Sodium-ion batteries, as large-scale energy storage systems, have been attracting much attention for application in EVs and stationary energy storage systems because of the abundant resources and low cost of sodium [1-3]. Although sodium-ion batteries are being studied since the past three decades [4], extensive efforts have been devoted to develop lithium-ion batteries because of their high

energy density. For practical application of sodium-ion batteries, it is necessary to develop new electrode materials with high capacities, good rate capabilities, and long cycle lives.

In recent years, many materials, including alloy materials [5-8], carbon materials [9-12], and transition metal oxide materials [13-18], have been investigated as negative electrode materials for sodium-ion batteries. Among them, transition metal oxides are attracting increasing attention due to their high volume capacities and safety. The reaction mechanism of transition metal oxides with Na generally differs from the classical Na insertion/extraction or Na-alloying processes. It usually involves the reduction and oxidation of the transition metal, leading to the formation and decomposition of Na_2O, which can give a relatively high theoretical capacity because of the multiple electron exchange per transition metal. $NiCo_2O_4$ was the first negative electrode material to be investigated; it afforded a reversible capacity of 200 mAh g^{-1} with a first charge capacity of 618 mAh g^{-1} and the formation of metallic Ni and Co [13]. Fe_2O_3 has also been used as a negative electrode material with high reversible capacities of 420–550 mAh g^{-1} in organic electrolytes [14,16,19]; however, their cycle performance was relatively poor. Co_3O_4 was reported to have reversible capacities of 440–516 mAh g^{-1} in the voltage range of 0.01–3.0 V [20,21]. MoO_3 was also investigated as a high-performance negative electrode material and showed a reversible capacity of 410 mAh g^{-1} in the voltage range of 0.04–3.0 V [22]. However, both Co_3O_4 and MoO_3 exhibit relatively poor cycle performance.

Recently, anatase TiO_2 was investigated as a negative electrode material and showed reversible capacities of 193–275 mAh g^{-1} and good cycle stability [17,23]. In terms of earth-abundance and environmental friendliness, Ti-based and Fe-based transition metal oxides are promising negative electrode materials for sodium-ion batteries. In view of the advantages of TiO_2 and Fe_2O_3, new negative electrode materials can be developed by combining them. In this study, we develop a negative electrode material comprising $FeTiO_3$ for sodium-ion batteries. To improve the electrochemical performance, nanostructuring and carbon-coating are also used.

Yu et al. recently reported a $FeTiO_3$-based negative electrode with tiny ilmenite $FeTiO_3$ nanoparticle embedded carbon nanotubes (carbon content: 28.69 wt%), which presents an excellent cycle stability and remarkable rate capability [24]. This indicates that the addition of carbon can effectively improve the electrochemical performance of $FeTiO_3$. However, the carbon content is relatively high in the $FeTiO_3$ nanoparticle embedded carbon nanotubes. In this work, we synthesize carbon-coated $FeTiO_3$ ($FeTiO_3$/C) nanoparticles with low carbon content and report for the first time the charge-discharge performance of $FeTiO_3$/C electrodes for sodium-ion batteries in ionic liquid electrolyte at 90 °C. Ionic liquids have non-flammability, negligible volatility, high thermal and electrochemical stability, and relatively high ionic conductivity, and they have been regarded as promising electrolytes for sodium-ion batteries [23, 25-27]. Compared with the conventional organic electrolytes, ionic liquid electrolytes are very safe, especially at high temperatures. The use of ionic liquid electrolytes can solve the safety issue of sodium-ion batteries, especially for large-scale applications.

2. Experimental section

Commercial anatase TiO_2 nanoparticles (Sigma Aldrich, USA), $Fe(NO_3)_3 \cdot 9H_2O$ (Wako, Japan), and sucrose (Sigma Life Science, USA) were used as the raw materials to synthesize carbon-coated $FeTiO_3$ ($FeTiO_3$/C) nanoparticles. $Fe(NO_3)_3 \cdot 9H_2O$ was firstly dissolved in ethanol under stirring at the room temperature. TiO_2 nanoparticles were then dispersed in the $Fe(NO_3)_3$ solution with the molar ratio of 1:1 to form a suspension by magnetic stirring. After drying, the mixture of TiO_2 and $Fe(NO_3)_3$ was heated at 300 °C for 3 h in air. The obtained powders were then mixed with sucrose (10 wt% carbon) by a mortar and pestle. Finally, the mixture was heated in Ar atmosphere at 600 °C for 5 h to obtain $FeTiO_3$/C nanoparticles.

The crystal phase of the synthesized $FeTiO_3$/C nanoparticles was analyzed by X-ray diffraction (XRD; Rigaku SmartLab) using Cu $K\alpha$ radiation. The morphology of the synthesized $FeTiO_3$/C nanoparticles was observed by field emission scanning electron microscopy (FE-SEM; Hitachi SU8000) with energy dispersive X-ray spectroscopy (EDX) analysis. The carbon content of the $FeTiO_3$/C nanoparticles was measured by a CHN analyzer.

The electrochemical tests were performed using coin-type 2032 cells with a sodium foil as the counter electrode at 90 °C. The $FeTiO_3$/C electrodes were fabricated by a conventional coating method. A slurry consisting of $FeTiO_3$/C (80 wt%), acetylene black (10 wt%), and polyamide-imide (PAI) (10 wt%) in *N*-methyl-2-pyrrolidone (NMP) was uniformly spread onto an Al foil. The $FeTiO_3$/C electrodes were dried in vacuo at 120 °C overnight before transferring into an Ar-filled glovebox. The mass loading of $FeTiO_3$/C material was 0.8−1.3 mg cm^{-2}. The Na[FSA]-[C_3C_1pyrr][FSA] (FSA = bis(fluorosulfonyl)amide; C_3C_1pyrr = *N*-methyl-*N*-propylpyrrolidinium) ionic liquid was used as the electrolyte with a molar ratio of 2:8. The measuring temperature of 90 °C was adopted because the Na[FSA]-[C_3C_1pyrr][FSA] ionic liquid exhibits good ionic conductivity and low viscosity at high temperatures [26]. Glass fiber filters (Whatman, GF-A, 260 mm) were used as separators. The working electrodes and separators were vacuum-impregnated with the Na[FSA]-[C_3C_1pyrr][FSA] ionic liquid before assembling the cells. Charge-discharge testing was conducted at constant current rates of 10–2000 mA g^{-1} in the voltage range of 0.01–2.5 V. After the charge-discharge tests, the $FeTiO_3$/C electrodes were removed from the testing coin cells and were washed to remove the ionic liquid electrolyte by anhydrous tetrahydrofuran (THF; Wako Pure Chemicals) in an Ar-filled glovebox. The crystal structure and morphology of the $FeTiO_3$/C electrodes were investigated by XRD and SEM, where the $FeTiO_3$/C electrodes were sealed in an airtight sample holder to avoid air exposure.

3. Results and discussion

Figure 1a shows the XRD pattern of the synthesized $FeTiO_3$/C nanoparticles. All diffraction peaks are indexed to the ilmenite $FeTiO_3$ structure (JCPDS file No. 01-079-1838), indicating the formation of single-phase $FeTiO_3$. The average crystallite size of the $FeTiO_3$/C nanoparticles is ca. 30 nm according to the Scherrer's formula. The carbon content of the $FeTiO_3$/C nanoparticles was determined to be 4.8 wt% by a CHN analyzer. The SEM image of the synthesized $FeTiO_3$/C nanoparticles is shown in Fig. 1b. The average particle size of the $FeTiO_3$/C nanoparticles is less than 100 nm.

Figure 2a shows the charge-discharge curves of the $FeTiO_3$/C electrode at a current rate of 10 mA $(g\text{-}FeTiO_3/C)^{-1}$ in the voltage range of 0.01–2.5 V. In the first charge process, a large capacity of 834 mAh $(g\text{-}FeTiO_3/C)^{-1}$ was observed with two distinct voltage plateaus at around 1.6 V and 0.5 V. The plateau at 1.6 V is attributable to some side reactions, including the electrolyte reduction and formation of a solid-electrolyte interphase [23,28], and it disappears in the subsequent cycles. The voltage plateau at 0.5 V possibly corresponds to the insertion of Na ions into $FeTiO_3$/C. In the first discharge process, there are two voltage plateaus at ca. 0.8 V and 1.7 V which correspond to extraction reaction of Na ions from $FeTiO_3$/C electrode, giving a discharge capacity of 390 mAh $(g\text{-}FeTiO_3/C)^{-1}$. The observed high irreversible capacity of 444 mAh $(g\text{-}FeTiO_3/C)^{-1}$ in the first cycle is obviously the biggest challenge for the practical application of the $FeTiO_3$/C electrodes. Nevertheless, this problem can probably be resolved by using appropriate conducting agents other than acetylene black (AB), because the high irreversible capacity likely originates from the side reactions between the electrolyte and AB (Fig. S1, Supporting Information). In the second cycle, the electrode exhibits a high reversible capacity of 403 mAh $(g\text{- }FeTiO_3/C)^{-1}$, which corresponds to approximately 76% of the theoretical capacity based on a three-electron reaction (530 mAh g^{-1}). In the subsequent cycles,

a remarkably stable charge-discharge behavior is observed. The reversible capacity of the $FeTiO_3$/C electrode is similar to that (about 410 mAh g^{-1}) reported for the $FeTiO_3$-based negative electrode with tiny ilmenite $FeTiO_3$ nanoparticle embedded carbon nanotubes in an organic electrolyte at 25 °C [24]. For comparison, charge-discharge measurements were also conducted for the $FeTiO_3$/C electrode at 25 °C in the ionic liquid electrolyte and an organic electrolyte (1 M $NaPF_6$ in ethylene carbonate/dimethyl carbonate (EC-DMC, 1:1 in volume)). As shown in Fig. S2 (Supporting Information), the $FeTiO_3$/C electrode exhibits a reversible capacity of about 120 mAh g^{-1} in the ionic liquid at 25 °C. The capacity is lower than that at 90 °C because of the high viscosity and low conductivity of the ionic liquid at 25 °C [26]. Thus, the $FeTiO_3$/C electrode in the ionic liquid electrolyte is suitable to be operated at high temperature. In the $NaPF_6$/EC-DMC electrolyte at 25 °C, the reversible capacity is about 150 mAh g^{-1}, which is lower than that measured in the ionic liquid at 90 °C. The value is also lower than that reported for the $FeTiO_3$-based electrode in an organic electrolyte at 25 °C [24]. The low discharge capacity in the $NaPF_6$/EC-DMC at 25 °C may be attributed to the poor compatibility with PAI binder. The combination of $FeTiO_3$/C, PAI binder and $NaPF_6$/EC-DMC does not seem to be suitable for high performance because some change has occurred on the electrode after measurement. Further optimization of electrode is needed to improve the charge-discharge performance of the $FeTiO_3$/C electrode in the organic electrolyte at 25 °C.

Rate capability is also an important parameter to characterize the electrochemical performance. Figure 2b shows the charge-discharge curves of the $FeTiO_3$/C electrode at current rates of 10–2000 mA g^{-1}. Although the polarization between the charge and discharge processes increases with the increasing current rate, the shape of the charge-discharge curves remains almost unchanged. Figure 2c shows the discharge capacities of the $FeTiO_3$/C electrode at different current rates. At a current rate of 200 mA g^{-1}, the discharge capacity is 326 mAh g^{-1}, which corresponds to 81% of the discharge capacity at 10 mA g^{-1}. When the current rate

increases to 2000 mA g^{-1}, the discharge capacity is 256 mAh g^{-1}, which corresponds to 64% of the discharge capacity at 10 mA g^{-1}. Thus, the $FeTiO_3$/C electrode is confirmed to have a good rate capability.

Cycle performance is another important parameter, especially for practical application of the $FeTiO_3$/C electrodes. Figure 2d shows the cycle performance of the $FeTiO_3$/C electrode at a current rate of 500 mA g^{-1} for 2000 cycles. In the first cycle, the discharge capacity is 241 mAh g^{-1} with a coulombic efficiency of 55.8%. The discharge capacity increases gradually with the cycle number, and reaches 275 mAh g^{-1} at the 200th cycle with a coulombic efficiency of 99.9%. After 500, 1000, 1600, and 2000 cycles, the discharge capacities are 280, 282, 280, and 274 mAh g^{-1}, respectively, with coulombic efficiencies higher than 99.9%. As far as we know, such excellent cycle performance has never been reported for transition metal oxide materials.

Table 1 compares the reversible capacities, cycle performance and high rate capacities of the negative electrode materials reported so far as well as the $FeTiO_3$/C. Alloying materials, such as Sn [29] and SnSb/C [30], show high reversible capacities of larger than 500 mAh g^{-1}, which is higher than that of the $FeTiO_3$/C (403 mAh g^{-1}). However, due to the volume expansion correlated with the structure destruction of the electrodes during cycling, the alloying materials generally exhibit poor cycle performance and low rate capability. Compared with the alloy electrodes, the $FeTiO_3$/C negative electrode shows excellent cycle performance and higher rate capability. Carbon materials, such as hard-carbon [31], carbon black [32] and hollow carbon [33], deliver reversible capacities of 200-300 mAh g^{-1} with relatively good cycle performance and rate capability. Compared with the carbon materials, the $FeTiO_3$/C negative electrode shows higher reversible capacity, better cycle performance and higher rate capability. Among oxide electrode materials, Fe_2O_3/C [19], Co_3O_4/C [21], MoO_3 [22], SnO_2 [34], and $NiCo_2O_4$/C [35] exhibit reversible capacities of higher than 400 mAh g^{-1}, exceeding the capacity of the $FeTiO_3$/C. Concerning the titanium-based oxides, TiO_2/C [23], $NaFeTiO_4$ [36], $Na_2Ti_3O_7$ [37] and

$Na_2Ti_6O_{13}$ [38] show reversible capacities of less than 300 mAh g^{-1}, which is lower than that of the $FeTiO_3$/C. Compared with the reported oxide materials, the $FeTiO_3$/C negative electrode shows better cycle performance and higher rate capability. In comparison with the $FeTiO_3$-based negative electrode with tiny ilmenite $FeTiO_3$ nanoparticle embedded carbon nanotubes (carbon content: 28.69 wt%) [24], the $FeTiO_3$/C (carbon content: 4.8 wt%) negative electrode exhibits almost the same reversible capacity and the high rate capability. Concerning the cycle retention, however, the $FeTiO_3$/C negative electrode (97 % after 2000 cycles) shows higher performance than the tiny ilmenite $FeTiO_3$ nanoparticle embedded carbon nanotubes (90% after 2000 cycles [24]). Thus, the $FeTiO_3$/C is concluded to be a promising negative material for sodium-ion batteries because of its high reversible capacity, excellent cycle performance and high rate capability.

The electrochemical sodiation-desodiation mechanism for the $FeTiO_3$/C electrode was analyzed by ex situ XRD, as shown in Fig. 3. During the charge process (sodiation), the pristine $FeTiO_3$ crystal phase gradually disappears. There is no significant change in the XRD pattern for the pristine electrode (electrode-1) and 0.8 V-charged electrode (electrode-2), except for the peak intensity. While charging to 0.5 V (electrode-3), a second phase grows at the expense of the pristine one. Here, the pristine $FeTiO_3$ crystal phase is still detectable with a weak peak intensity. When the electrode is charged to 0.01 V (electrode-5), the pristine $FeTiO_3$ crystal phase completely disappears and only the new crystal phase is detected. Since the new crystal phase is very similar to $Na_{0.54}TiO_2$ (JCPDS file No. 01-080-1053) (Fig. S3a, Supporting Information), the Na_xTiO_2 ($0.5 < x < 1$) crystal phase is likely formed in the charged electrode. If Na_xTiO_2 is formed, the metallic Fe phase should be generated. However, no Fe crystal phase is detected in the XRD pattern, indicating that the formed Fe phase is amorphous. To investigate the oxidation state of Fe atoms, X-ray photoelectron spectroscopy (XPS) was carried out for the electrode charged to 0.01 V. As shown in Fig. S4 (Supporting Information), Fe^{2+} and Fe^0

are present in the charged electrode, indicating the formation of amorphous Fe formed in the electrode. In addition, according to the sodiation mechanism of Fe_2O_3, where Fe_2O_3 is converted into Fe and Na_2O [14,16], Na_2O should be formed in the charged electrode.

During the discharge process (desodiation), from electrode-5 to electrode-10, the formed Na_xTiO_2 crystal phase gradually disappears, and other crystal phase is formed. The formed crystal phase in electrode-10 is well consistent with the $FeTiO_3$ crystal phase (Fig. S3b, Supporting Information), indicating the recovery of the pristine $FeTiO_3$ crystal phase during the desodiation process. XPS analysis of electrode-10 also shows that the main oxidation state of Fe is Fe^{2+} (Fig. S4, Supporting Information). Thus, the reversible sodiation-desodiation reaction is summarized as follows: in the charging process, Na ions are electrochemically reduced and react with $FeTiO_3$ to form Na_xTiO_2, Fe, and Na_2O; in the discharging process, the products are converted back to $FeTiO_3$ and Na ions. The highly reversible sodiation/desodiation processes, in addition to the carbon coating, contribute to the excellent cycle performance of the $FeTiO_3$/C electrode.

To investigate the microscopic morphological changes of the $FeTiO_3$/C electrodes during the sodiation-desodiation processes, ex situ SEM analysis was carried out and the results are shown in Fig. 4. For reference, the SEM image of a pristine electrode is shown in Fig. 4a. When the electrode is charged to 0.5 V, some round particles form on the surface (Fig. 4b). These round particles grow in size when being charged to 0.01 V (Fig. 4c), and are still present when the electrode is discharged to 2.5 V (Fig. 4d). Since the formation of round particles is irreversible, the formation is likely due to the electrolyte reduction in the first charge process, as shown in Figure 2a. The formation of round particles has been also observed for the TiO_2/C electrode in the same electrolyte, where the energy dispersive X-ray analysis of the round particles reveals that it resulted from electrolyte reduction [28]. In addition, the electrode charged to 0.01 V has some needle-like particles (Fig. 4c). When the electrode is discharged to 2.5 V, the needle-like

particles disappear (Fig. 4d), indicating that the formation of these particles is reversible.

4. Conclusions

In summary, we have reported $FeTiO_3$/C as a negative electrode material for sodium-ion batteries. The $FeTiO_3$/C electrode exhibits a high reversible capacity of 403 mAh g^{-1} with outstanding cycling stability for up to 2000 cycles. We have also elucidated the sodiation-desodiation mechanism of the $FeTiO_3$/C electrode. These results have the potential to greatly contribute toward the development of sodium-ion batteries. We also believe that our results can provide a guidepost for exploring new negative electrode materials for sodium-ion batteries with high energy density and long cycle lives.

Acknowledgements

This study was partly supported by the Advanced Low Carbon Technology Research and Development Program (ALCA, No. 3428) of the Japan Science and Technology Agency (JST), and the "Elements Strategy Initiative to Form Core Research Center" program of the Japanese Ministry of Education, Culture, Sports, Science and Technology (MEXT).

References

[1] N. Yabuuchi, M. Kajiyama, J. Iwatate, H. Nishikawa, S. Hitomi, R. Okuyama, R. Usui, Y. Yamada, S. Komaba, *Nat. Mater.* 11 (2012) 512-517.

[2] S. W. Kim, D. H. Seo, X. H. Ma, G. Ceder, K. Kang, *Adv. Energy Mater.* 2 (2012) 710-721.

[3] V. Palomares, P. Serras, I. Villaluenga, K. B. Hueso, J. Carretero-Gonzalez, T. Rojo, *Energy Environ. Sci.* 5 (2012) 5884-5901.

[4] K. M. Abraham, *Solid State Ionics* 7 (1982) 199-212.

[5] L. Wu, X. H. Hu, J. F. Qian, F. Pei, F. Y. Wu, R. J. Mao, X. P. Ai, H. X. Yang, Y. L. Cao, *Energy Environ. Sci.* 7 (2014) 323-328.

[6] Y. H. Liu, Y. H. Xu, Y. J. Zhu, J. N. Culver, C. A. Lundgren, K. Xu, C. S. Wang, *ACS Nano* 7 (2013) 3627-3634.

[7] X. Q. Xie, K. Kretschmer, J. Q. Zhang, B. Sun, D. W. Su, G. X. Wang, *Nano Energy* 13 (2015) 208-217.

[8] Y. H. Xu, Y. J. Zhu, Y. H. Liu, C. S. Wang, *Adv. Energy Mater.* 3 (2013) 128-133.

[9] S. Komaba, W. Murata, T. Ishikawa, N. Yabuuchi, T. Ozeki, T. Nakayama, A. Ogata, K. Gotoh, K. Fujiwara, *Adv. Funct. Mater.* 21 (2011) 3859-3867.

[10] J. Zhao, L. W. Zhao, K. Chihara, S. Okada, J. Yamaki, S. Matsumoto, S. Kuze, K. Nakane, *J. Power Sources* 244 (2013) 752-757.

[11] J. Ding, H. L. Wang, Z. Li, A. Kohandehghan, K. Cui, Z. W. Xu, B. Zahiri, X. H. Tan, E. M. Lotfabad, B. C. Olsen, D. Mitlin, *ACS Nano* 7 (2013) 11004-11015.

[12] Y. L. Cao, L. F. Xiao, M. L. Sushko, W. Wang, B. Schwenzer, J. Xiao, Z. M. Nie, L. V. Saraf, Z. G. Yang, J. Liu, *Nano Lett.* 12 (2012) 3783-3787.

[13] R. Alcantara, M. Jaraba, P. Lavela, J. L. Tirado, *Chem. Mater.* 14 (2002) 2847-2848.

[14] Y. Z. Jiang, M. J. Hu, D. Zhang, T. Z. Yuan, W. P. Sun, B. Xu, M. Yan, *Nano Energy* 5 (2014) 60-66.

[15] I. Hasa, R. Verrelli, J. Hassoun, *Electrochim. Acta* 173 (2015) 613-618.

[16] M. Valvo, F. Lindgren, U. Lafont, F. Bjorefors, K. Edstrom, *J. Power Sources* 245 (2014) 967-978.

[17] K. T. Kim, G. Ali, K. Y. Chung, C. S. Yoon, H. Yashiro, Y. K. Sun, J. Lu, K. Amine, S. T. Myung, *Nano Lett.* 14 (2014) 416-422.

[18] J. C. Perez-Flores, C. Baehtz, A. Kuhn, F. Garcia-Alvarado, *J. Mater. Chem. A* 2 (2014) 1825-1833.

[19] Z. L. Jian, B. Zhao, P. Liu, F. J. Li, M. B. Zheng, M. W. Chen, Y. Shi, H. S. Zhou, *Chem. Commun.* 50 (2014) 1215-1217.

[20] M. M. Rahman, A. M. Glushenkov, T. Ramireddy, Y. Chen, *Chem. Commun.* 50 (2014) 5057-5060.

[21] Y. Wang, C. Y. Wang, Y. J. Wang, H. K. Liu, Z. G. Huang, *J. Mater. Chem. A* 4 (2016) 5428-5435.

[22] S. Hariharan, K. Saravanan, P. Balaya, *Electrochem. Commun.* 31 (2013) 5–9.

[23] C. S. Ding, T. Nohira, R. Hagiwara, *J. Mater. Chem. A* 3 (2015) 20767-20771.

[24] L. Yu, J. Liu, X. Xu, L. Zhang, R. Hu, J. Liu, L. Ouyang, L. Yang, M. Zhu, *ACS Nano* 11 (2017) 5120-5129.

[25] C. S. Ding, T. Nohira, K. Kuroda, R. Hagiwara, A. Fukunaga, S. Sakai, K. Nitta, S. Inazawa, *J. Power Sources* 238 (2013) 296–300.

[26] C. S. Ding, T. Nohira, R. Hagiwara, K. Matsumoto, Y. Okamoto, A. Fukunaga, S. Sakai, K. Nitta, S. Inazawa, *J. Power Sources* 269 (2014) 124-128.

[27] G. A. Giffin, *J. Mater. Chem. A* 4 (2016) 13378-13389.

[28] C. S. Ding, T. Nohira, R. Hagiwara, *Phys. Chem. Chem. Phys.* 18 (2016) 30770-30776.

[29] Y. M. Lin, P. R. Abel, A. Gupta, J. B. Goodenough, A. Heller, C. B. Mullins, *ACS Appl. Mater. Interfaces* 5 (2013) 8273−8277.

[30] L. Xiao, Y. Cao, J. Xiao, W. Wang, L. Kovarik, Z. Nie, J. Liu, *Chem. Commun.* 48 (2012) 3321-3323.

[31] C. S. Ding, T. Nohira, R. Hagiwara, A. Fukunaga, S. Sakai, K. Nitta, *Electrochim. Acta* 176 (2015) 344–349.

[32] W. Xiao, Q. Sun, J. Liu, B. Xiao, P. Glans, J. Li, R. Li, J. Guo, W. Yang, T. Sham, X. Sun, *Nano Res.*, 2017, https://doi.org/10.1007/s12274-017-1852-4.

[33] Y. L. Cao, L. F. Xiao, M. L. Sushko, W. Wang, B. Schwenzer, J. Xiao, Z. M. Nie, L.V. Saraf, Z. G. Yang, J. Liu, *Nano Lett.* 12 (2012) 3783-3787.

[34] D. Su, C. Wang, H. Ahn, G. Wang, *Phys. Chem. Chem. Phys.* 15 (2013) 12543-12550.

[35] Y. Wang, H. Huang, Q. Xie, Y. Wang, B. Qu, *J. Alloys Compounds* 705 (2017) 314-319.

[36] J. Wang, B. Qiu, X. He, T. Risthaus, H. D. Liu, M. C. Stan, S. Schulze, Y. G Xia, Z. P. Liu, M. Winter, J. Li, *Chem. Mater.* 27 (2015) 4374−4379.

[37] A. Rudola, K. Saravanan, C.W. Mason, P. Balaya, *J. Mater. Chem. A* 1 (2013) 2653-2662.

[38] A. Rudola, K. Saravanan, S. Devaraj, H. Gong, P. Balaya, *Chem. Commun.* 49 (2013) 7451 -7453.

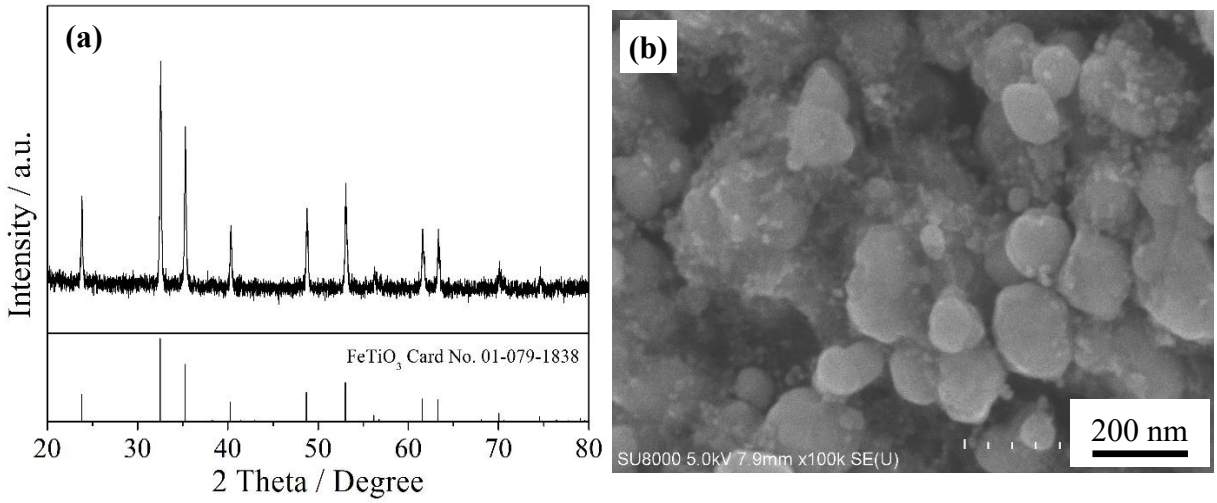

Fig. 1 (a) XRD pattern and (b) SEM image of $FeTiO_3$/C nanoparticles.

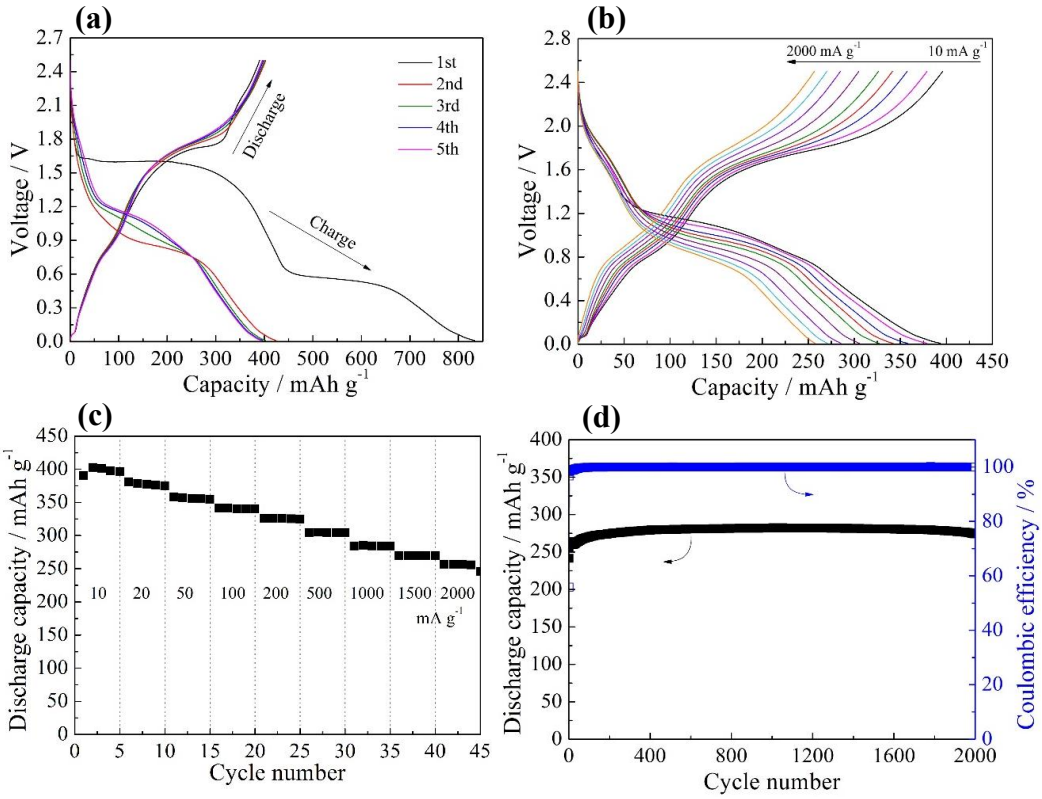

Fig. 2 Electrochemical performance of $FeTiO_3$/C electrode. (a) Charge-discharge curves at a current rate of 10 mA g^{-1} in the voltage range of 0.01–2.5 V. (b) Charge-discharge curves at current rates of 10, 20, 50, 100, 200, 500, 1000, 1500, and 2000 mA g^{-1}. (c) Rate capability. d) Cycle performance at a current rate of 500 mA g^{-1}.

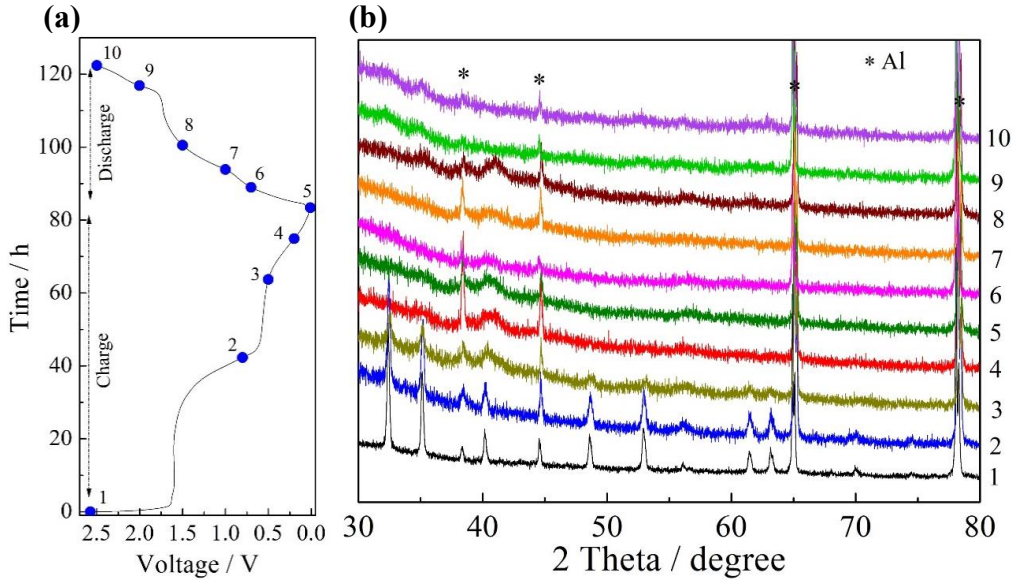

Fig. 3 Electrochemical and structural characterization of the $FeTiO_3$/C electrode. a) Charge-discharge curves at 10 mA g^{-1} in the first cycle. The numbers indicate the charged and discharged states of the $FeTiO_3$/C electrode. b) Ex situ XRD patterns of the $FeTiO_3$/C electrode at various charge/discharge stages: (1) pristine electrode, (2) electrode charged to 0.8 V, (3) electrode charged to 0.5 V, (4) electrode charged to 0.2 V, (5) electrode charged to 0.01 V, (6) electrode discharged to 0.7 V, (7) electrode discharged to 1.0 V, (8) electrode discharged to 1.5 V, (9) electrode discharged to 2.0 V, and (10) electrode discharged to 2.5 V, as indicated in (a).

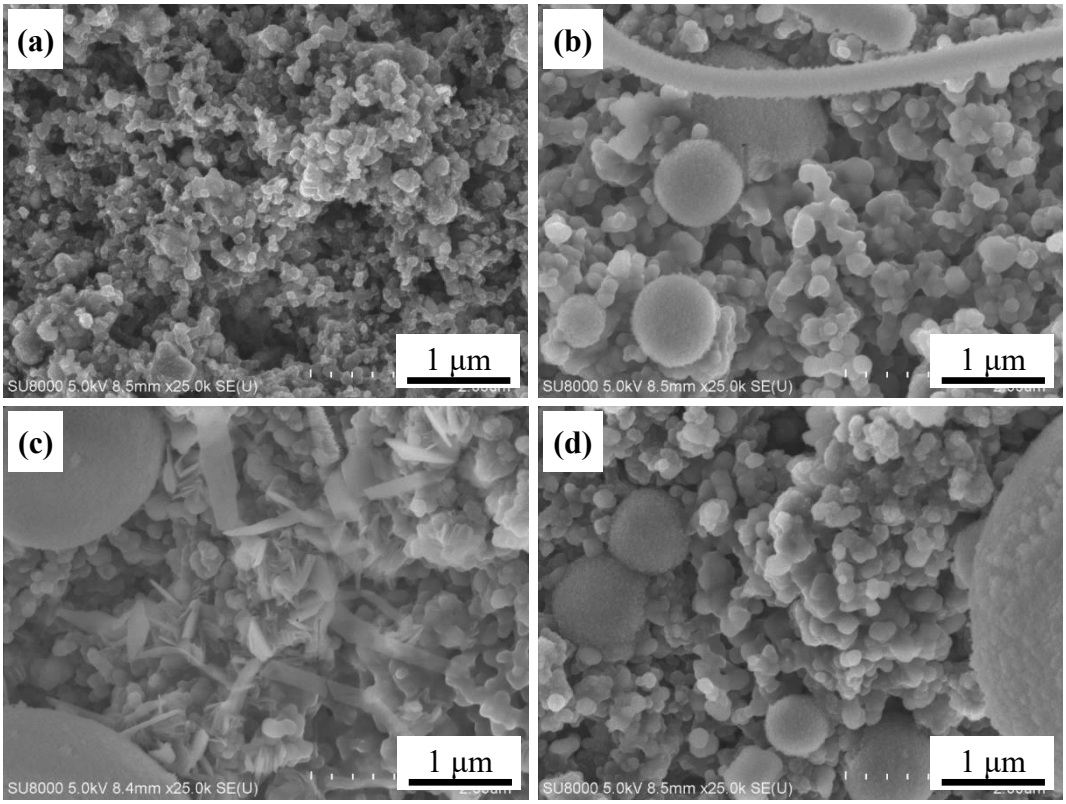

Fig.4 SEM observation of $FeTiO_3$/C electrodes with different charge-discharge states. a) Pristine electrode. b) Electrode charged to 0.5 V. c) Electrode charged to 0.01 V. d) Electrode discharged to 2.5 V.

Table 1 Electrochemical performance of negative electrode materials reported so far for sodium-ion batteries.

Electrode materials	Reversible capacity (mAh g^{-1})	Cycle retention (%) after N cycles				High rate capacity (mAh g^{-1}) (rate (mA g^{-1}))	Reference
		100	500	1000	2000		
Sn	510	49	-	-	-	222 (422)	29
SnSb/C	544	80*	-	-	-	274 (1000)	30
Hard carbon	277	94	84	-	-	230 (1000)	31
Carbon black	234	79	57	56	57	159 (400)	32
Hollow carbon	251	90	82**	-	-	149 (500)	33
TiO_2/C	275	91	89	79	-	174 (500)	23
SnO_2	510	85	-	-	-	250 (160)	34
Co_3O_4/C	516	94	80	67	-	263 (1000)	21
MoO_3	410	88	55	-	-	158 (559)	22
Fe_2O_3/C	535	77	-	-	-	260 (500)	19
$NiCo_2O_4$/C	440	90	-	-	-	180 (800)	35
$NaFeTiO_4$	181	99	98	-	-	68 (354)	36
$Na_2Ti_3O_7$	177	65*	-	-	-	100 (356)	37
$Na_2Ti_6O_{13}$	42	89	87	-	-	15 (495)	38
$FeTiO_3$-carbon nanotubes	410	99	96	96	90	273 (1000)	24
$FeTiO_3$/C	403	99	99	99	97	285 (1000)	This study

* 50 cycles ** 400 cycles